

We are IntechOpen, the world's leading publisher of Open Access books Built by scientists, for scientists

6,900

Open access books available

186,000

International authors and editors

200M

Downloads

Our authors are among the

154

Countries delivered to

TOP 1%

most cited scientists

12.2%

Contributors from top 500 universities



WEB OF SCIENCE™

Selection of our books indexed in the Book Citation Index
in Web of Science™ Core Collection (BKCI)

Interested in publishing with us?
Contact book.department@intechopen.com

Numbers displayed above are based on latest data collected.
For more information visit www.intechopen.com



Chapter

Transition Metals Doped Nanocrystals: Synthesis, Characterization, and Applications

Anielle C.A. Silva, Jerusa M. de Oliveira, Luciana R.S. Floresta, Matheus V. da Silva, José L. da S. Duarte, Karolina B. da Silva, Eurípedes A. da Silva Filho, Vinícius P. Bittar, Ana L.S. Borges, Guilherme L. Fernandes, Alessandra S. Silva, Éder V. Guimarães, Ricardo S. Silva, Carmem L.P.S. Zanta, Lucas Anhezini and Noelio O. Dantas

Abstract

Doping is a technique that makes it possible to incorporate substitutional ions into the crystalline structure of materials, generating exciting properties. This book chapter will comment on the transition metals (TM) doped nanocrystals (NCs) and how doping and concentration influence applications and biocompatibility. In the NCs doped with TM, there is a strong interaction of sp-d exchange between the NCs' charge carriers and the unpaired electrons of the MT, generating new and exciting properties. These doped NCs can be nanopowders or be embedded in glass matrices, depending on the application of interest. Therefore, we show the group results of synthesis, characterization, and applications of iron or copper-doped ZnO nanopowders and chromium-doped Bi₂S₃, nickel-doped ZnTe, and manganese-doped CdTe quantum dots in the glass matrices.

Keywords: Transition metals, Nanocrystals, Doping, Applications, Biocompatibility

1. Introduction

In view of the recent growth of the world population and the need for the suitable use and recycling of natural resources, emerging technologies have been continually called upon to present opportunities to address these global challenges. Expanding the benefits and reducing the risks for all, main principle of the planet's sustainability [1].

Metallic nanomaterials have been introduced as emerging technologies to respond to some of the aforementioned challenges. For example, iron and copper nanoparticles (NPs) have been utilized as plant micronutrients. Therefore, due to their success as antifungal and antibacterial, silver NPs have been applied to control phytopathogens and extend the vase life of some flowers [2]. Metallic NPs have also been used as nano-pesticides to increase the dispersion and wettability of agricultural formulations and unwanted pesticide movement [1, 3].

Besides the above mentioned, while some metallic NPs may have positive effects upon plant systems, it is also possible that this class of NPs has negative implications for plant systems. For instance, barriers to growth for plant systems may occur, negative impact soil microbial structure or function, directly or indirectly alter the formation of symbiotic associations with root fungi and bacteria, influencing nutrient availability and uptake, and plant growth [1].

A nanomaterial gaining popularity is zinc oxide (ZnO), the third metal-containing nanomaterial most commonly used [4–6]. The ZnO nanoparticle is considered multifunctional because it has high chemical stability, wide ultraviolet radiation absorption range and high photostability, and antifungal activity. Such properties allow this nanoparticle to be used to manufacture clothes with ultraviolet (UV) filters, sunscreens, baby rash ointments, paints, and even as food preservatives [7].

The ZnO NPs wide spectrum of applications makes it susceptible to entering the environment through various paths, such as effluents, spillage during transport, handling, direct contact through topical and oral consumer products, and incorrect disposal [8]. Such factors lead to contamination of environments and consequently adverse effects for humans and animals, such as excessive induction of reactive species, which can cause oxidative stress and trigger a cascade of damage in macromolecules, genotoxicity, apoptosis, neurotoxicity, and negative implications for embryonic development [9, 10]. We have shown that amorphous zinc oxide nanoparticles have greater genotoxicity than crystalline (nanocrystals - NCs) [11]. Besides, we have demonstrated its biocompatibility through intraosseous implants [12]. However, the search for nanomaterials with hybrid properties has been standing out even more in recent years.

Doping is a technique that makes it possible to incorporate substitutional ions into the crystalline structure of materials, generating exciting properties [13]. The transition metals are elements whose corresponding atoms do not have a more energetic “d” orbital filled or capable of forming cations with an incomplete d orbital. Therefore, the incorporation of these metals in nanocrystals makes it possible to mix properties, such as magneto-optics [refs]. In addition to this property, other properties are observed, some of which we will show in this chapter. In particular, we will show results of pure ZnO nanocrystals and doped with transition metals and that depending on the dopant, specific properties may or not be improved.

Depending on the doping ion, the nanoparticles’ toxicity may be reduced [14]. Copper (Cu) is one of the transition metals with the lowest toxicity to humans, which allows its application in medicine when used in intrauterine devices, and its antibacterial activity [14, 15]. Thus, in the present work, the ZnO NCs were doped with the copper transition metal (Cu doped ZnO) and reduction of toxicity due to doping. To evaluate the biocompatibility of this new nanoparticle, we analyzed the development of the fruit fly (*Drosophila melanogaster*) in a medium containing ZnO or Cu doped ZnO.

Drosophila melanogaster, known as fruit fly, is a well-established model organism in several areas of science, including nanotoxicology [16]. It offers several mutant lines for a broad range of human diseases, has low cost and easy maintenance in the laboratory, and a short life cycle compared to other model organisms such as mammals and fish. These features make the fruit fly a great model for studies

that evaluate long-term and developmental effects, which is still poorly studied in nanotoxicology [16]. The fruit fly also has 77% of the conserved genes related to human diseases [17] and considerable similarities with humans in different physiological mechanisms [18]. In addition, the use of *Drosophila melanogaster* as a model organism in nanotoxicology studies respects the Three Rs concept (Replacement, Reduction, and Refinement) as recommended by the European Center for the Validation of Alternative Methods (ECVAM) [19].

In some technological applications, it is essential that the nanocrystals are embedded in resistant and thermally and chemically stable systems, so the glass systems are excellent hosts [20, 21]. These nanocrystals can be doped with transition metals, aiming for several applications, such as the production of light-emitting diodes, photodetectors, spintronic, and others [21–24]. Therefore, this chapter will comment on the group results of nanocrystals doped with transition metals in the host glass matrix and how the dopant concentration modulates these properties.

Therefore, this chapter shows how the incorporation of transition metals in nanocrystals can change their physical, chemical, and biological properties. In particular, iron or copper-doped ZnO nanopowders and chromium-doped Bi₂S₃ nickel-doped ZnTe, and manganese-doped CdTe in the host glass matrices.

1.1 Iron-doped ZnO nanocrystals: development and applications

An important application using nanoparticles comes from environmental remediation. The accelerated population growth and the deficiency in basic sanitation, and the growth of industrial and agricultural activities have produced an increase in the pollution of the environment due to the generation of large residues that, when improperly treated, present high toxicity. In addition to the classic problems associated with contamination by priority pollutants, there is currently a considerable concern involving micropollutants considered emerging due to the inefficiency in their removal in conventional sewage treatment systems, thus often found in natural waters.

Synthetic and natural estrogens, antibiotics, pesticides, among others, are considered emerging pollutants. The degradation of emerging pollutants by conventional processes is hampered due to low concentrations and their molecular complexity. Thus, the study of new treatment proposals becomes very relevant, such as the application of metallic nanoparticles and catalysts for the degradation of emerging pollutants.

Figure 1(a) shows the illustrative scheme of crystalline structure of ZnO and the substitutional incorporation of iron (Fe) ions in the nanocrystal. **Figure 1(b)** shows the removals of the pollutant as a function of reaction time, and the different domains studied. The ZnO:11Fe material obtained the highest percentage of degradation, around 74.74% removal, followed by the pure ZnO nanoparticle. It is observed that all materials have similar behavior in reducing the pollutant absorbance. In this case, the different proportions of iron-doped ZnO NCs did not produce relevant effects in terms of efficiency, with all nanomaterials studied showing close percentages and removal kinetics.

1.2 Copper-doped ZnO nanocrystals: development and biocompatibility

The availability of various nanomaterials is increasing significantly, and contact with them is inevitable. Thus, it is necessary to determine its direct impact on the human body and the environment. The oral administration route chosen for the in vivo bioassay allows the observation of natural responses of the organism, [25], and it is the most common form of exposure to the ZnO NC in humans [8].

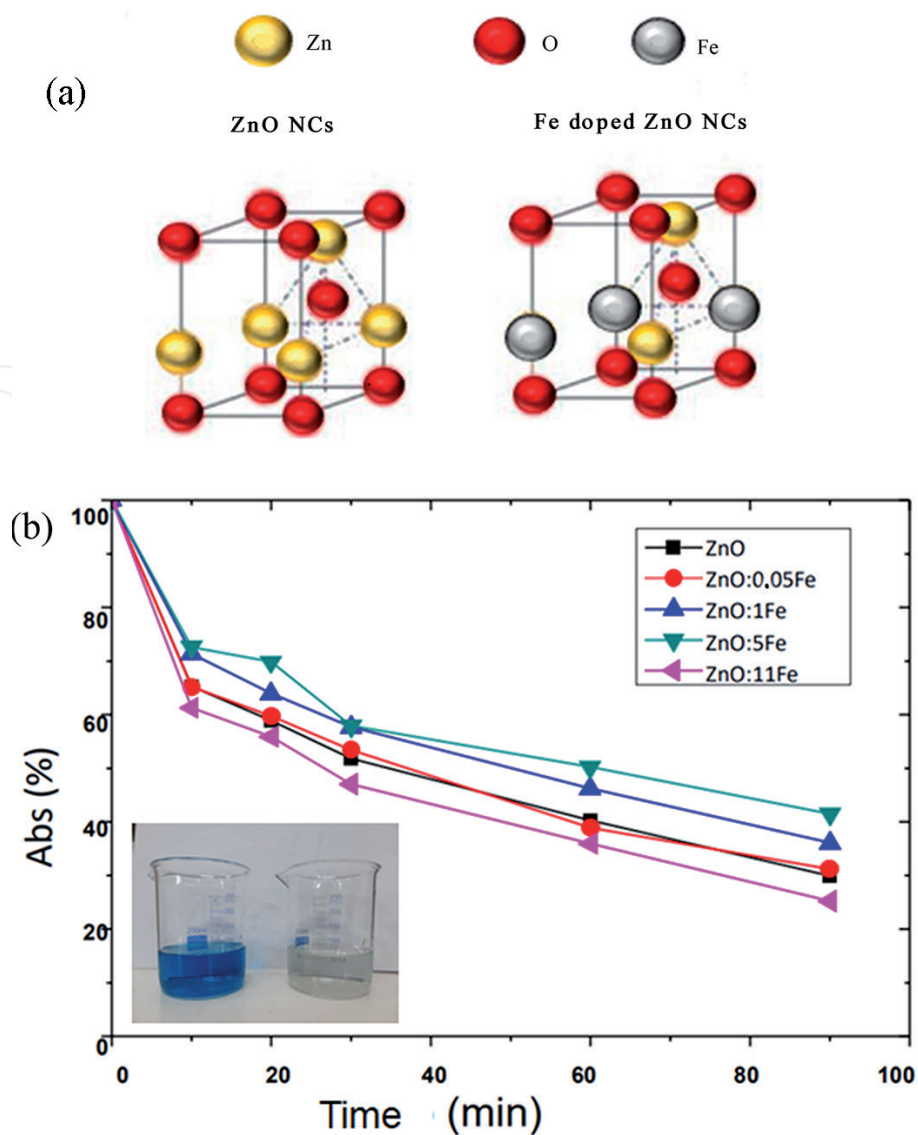


Figure 1.

(a) Illustrative scheme of the crystalline structure of ZnO and the substitutional incorporation of iron (Fe) ions in the nanocrystal. (b) Reduction of absorbance over time in reactions using Fe-doped ZnO in different proportions for malachite green degradation.

In this topic we present the toxicity analysis of pure and copper (Cu) doped ZnO NCs at a concentration of 0.25 mg/mL on the development of *Drosophila* larvae. **Figure 2(a)** shows the illustrative scheme of ZnO's crystalline structure and the substitutional incorporation of Cu ions in the nanocrystal. The results of the pupation rate following ZnO and Cu doped ZnO NCs exposure are shown in **Figure 2(b)**. As observed, there was a one-day delay in the time the larvae took to reach the pupal stage when exposed to Cu doped ZnO when compared to control and ZnO NCs (**Figure 2(c)**). Additionally, all the viable ZnO NCs treated animals were able to reach the puparium on the third day, while in the control samples, pupae formation was observed until the fifth day. Interestingly, most of the Cu doped ZnO NCs animals also reached the pupal stage on the fifth day. However, we could still observe pupae being formed until the eighth day. Delays in larval development were also evaluated in experiments carried out with *Drosophila* larvae that developed in medium containing silver (Ag) nanocrystals [26] or Cu on a nano or micrometric scale [27, 28]. In addition to the development delay analysis, we also observed the rate of larval lethality of the treated animals. The larvae developed at 0.25 mg/mL ZnO NCs showed the highest mortality rate when compared to control. Surprisingly, when ZnO NCs was copper doped (Cu doped ZnO) it reduced the

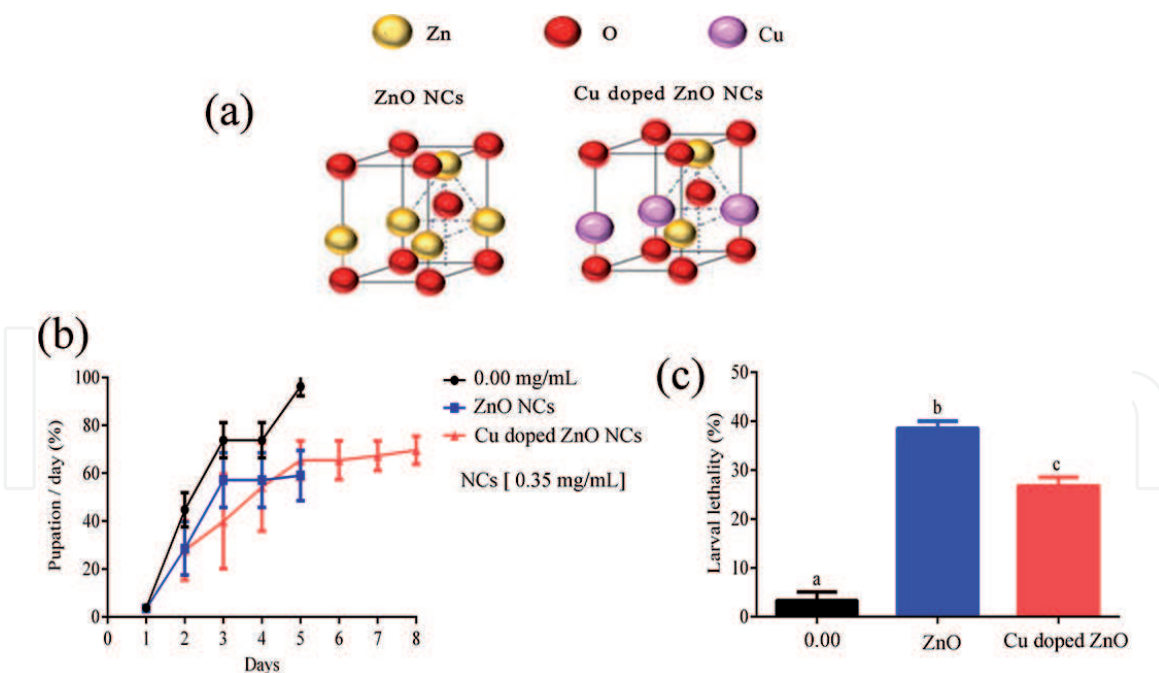


Figure 2. (a) Illustrative scheme of the crystalline structure of ZnO and the substitutional incorporation of Cu in the ZnO nanocrystal. The effects of ZnO and Cu doped ZnO NCs during the larval development of *Drosophila*. (b) Rate of daily pupal formation in animals treated with 0.25 mg/mL of ZnO or Cu doped ZnO. (c) Larval lethality rate after development in standard culture medium added with ZnO or Cu doped ZnO NCs. ($n = 6$; 35 larvae per replicate). abc indicates a statistical difference between treatments.

larval lethality by 12.5% compared to ZnO NCs, suggesting that copper doping was able to increase the ZnO NCs biocompatibility in vivo by decreasing its toxicity.

Developmental delays and lethality can be triggered by the formation of reactive species that cause redox imbalance and lead to cell damage, such as the oxidation of proteins, lipids, and DNA [9]. The redox imbalance leads to changes in the synthesis of antioxidants such as catalase (CAT), superoxide dismutase (SOD), glutathione S-transferase (GST), and the total glutathione (GSH) protein [29]. Total glutathione plays a crucial role in the synthesis of other antioxidant enzymes, such as GST, and is also involved in the ecdysone biosynthesis mechanism. Ecdysone plays various roles in the regulation of many developmental and physiological processes, especially molting and metamorphosis [30, 31]. Our data showed a high lethality and delay in larval development, which can be explained by the production of reactive species that initiate cellular damage and the imbalance of antioxidant enzymes. The imbalance in the synthesis of antioxidant enzymes, including GST, could lead to larval lethality and impair the ecdysone biosynthesis causing larval development problems. The decrease in larval lethality observed for Cu doped ZnO NCs compared to ZnO NCs could be explained by a lower effect on the level of antioxidant enzymes, suggesting that the transition metal copper was sufficient to increase ZnO NCs biocompatibility in vivo. However, additional studies are crucial to better understand the mechanisms by which development is influenced by nanocrystals.

1.3 Chrome-doped Bi₂S₃ nanocrystals embedded in host glass matrix

Diluted magnetic semiconductors (DMS) embedded in a glassy matrix, such as: Bi_{2-x}Mn_xS₃ [32], Bi_{2-x}Fe_xS₃, [33] Bi_{2-x}Co_xS₃ [34] and Bi_{2-x}Cr_xS₃, [35] have potential properties for the production of photovoltaic cells [36, 37] thermoelectric cooling, [38, 39] photodetectors, [40] field emission electronics [41] and fluorescent markers [42].

Bi₂S₃ (bulk) has an orthorhombic crystalline structure, [43] exciton Bohr radius of 24 nm [44], and bandgap of 1.3 eV [45]. The nature of the Cr S bond in Bi₂S₃ NCs

doped with Cr ions can lead to physical properties dependent on the spin dynamics, associated with the effects of quantum confinement of size, concentration control, and coordination site of the doping ions. As the Cr ions enter the Bi_2S_3 structure, replacing the Bi^{3+} ions, most likely with $3d^3$ valence and $3/2$ spin configurations, consequently, it becomes possible to add magnetic properties to the Bi_2S_3 non-magnetic NCs. The smaller ionic radius of Cr^{3+} (0.53 \AA) to Bi^{3+} (1.03 \AA) facilitates occupy vacancies in the Bi_2S_3 orthorhombic network [35, 46]. According to the theories of the crystal and ligand field, the energy states of the free Cr^{3+} ions will depend strongly on the interaction intensity of the chalcogenide ion (S^{2-}) environment that defines the crystal symmetry [34, 35, 46].

In this context, the role of x concentration of Cr ions in $\text{Bi}_{2-x}\text{Cr}_x\text{S}_3$ NCs incorporated in glassy systems, which derive from the control of charge carriers in the semiconductor energy bands, through the magnetic saturation of Cr^{3+} ions, was investigated to manipulate the properties of this new material.

Figure 3(a) shows the UV-VIS optical absorption spectra (OA) of $\text{Bi}_{2-x}\text{Cr}_x\text{S}_3$ NCs incorporated in SNAB glass matrix, at temperature (300 K), as a function of the increasing concentration of doping $x\text{Cr}$ ions ($x = 0.00; 0.050; 0.100$). The OA spectrum of the SNAB matrix (black line) appears at the bottom of **Figure 3(a)**. Throughout the spectral range, there is no band signal associated with the absorption of $\text{Bi}_{2-x}\text{Cr}_x\text{S}_3$ NCs. In comparison with the Bi_2S_3 NCs of the intrinsic semiconductor ($x = 0.00$), the OA spectra of the $\text{Bi}_{2-x}\text{Cr}_x\text{S}_3$ NCs underwent changes due to the doping of chromium ions in the symmetrical environment of

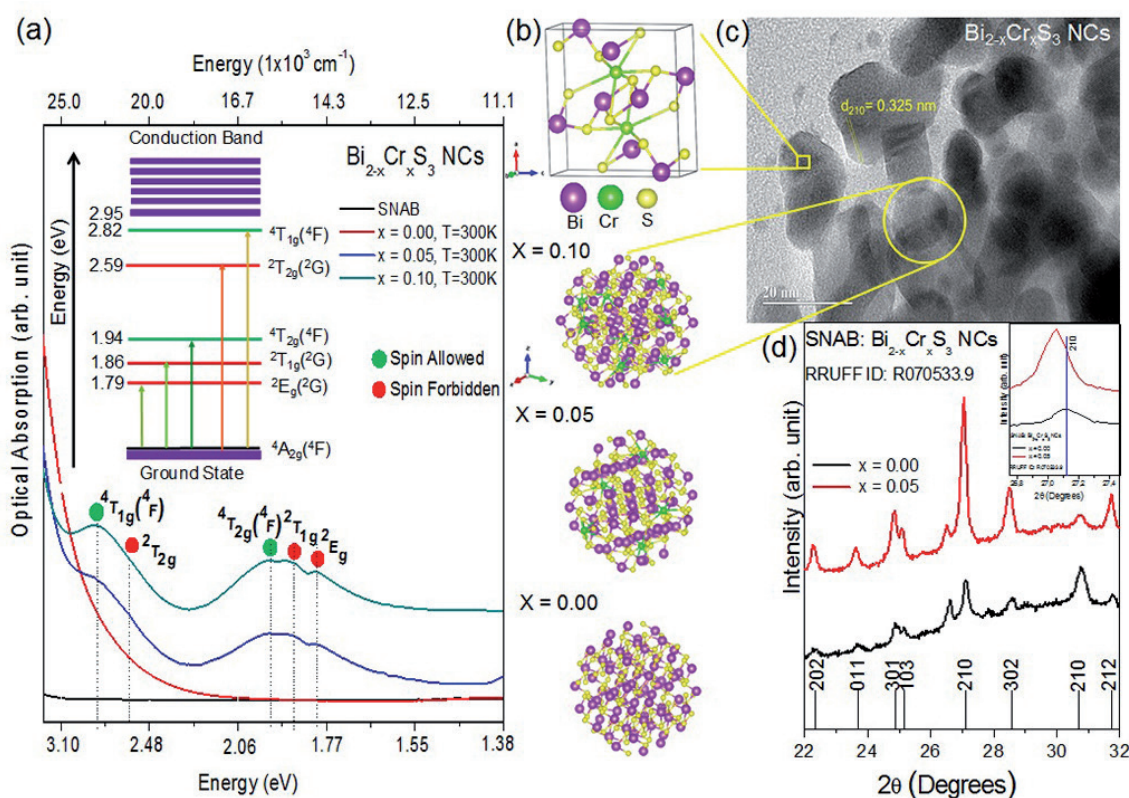


Figure 3.

(a) Optical absorption spectra at room temperature of $\text{Bi}_{2-x}\text{Cr}_x\text{S}_3$ NCs ($x = 0.00; 0.050$ and 0.100) incorporated in the SNAB glass matrix annealed for 2 h at 500°C . For comparison purposes, the absorption spectrum of the SNAB glass matrix is represented on the black bottom line. The insert shows the energy level diagram for Cr^{3+} ($3d^3$) at an octahedral site and the respective transitions allowed and prohibited by spin. (b) Bi_2S_3 orthorhombic unit cell and quantum dots with the interstitial replacement of Bi^{3+} ions by Cr^{3+} at distorted octahedral sites. (c) TEM images of $\text{Bi}_{2-x}\text{Cr}_x\text{S}_3$ NCs ($x = 0.10$). (d) XRD diffractograms at room temperature of $\text{Bi}_{2-x}\text{Cr}_x\text{S}_3$ NCs embedded in the SNAB glass matrix. The insertion shows a comparison between peaks (210) with increasing concentration x .

the NCs structure. The intensities of the electronic transition bands increased due to the increasing concentration of Cr^{3+} ions. Therefore, the OA spectra show energy bands of the components of the excitonic states and of the Cr^{3+} ions in the $\text{Bi}_{2-x}\text{Cr}_x\text{S}_3$ NCs.

According to the crystal field theory, the identified bands attributed to the Cr^{3+} ions correspond to the spin allowed and forbidden d-d transitions. The results presented in **Figure 3(a)** are evidence of the incorporation of Cr^{3+} ions in a ligand field of S^{2-} ions in octahedral coordination sites ($[\text{CrS}_6]^{-9}$) of the orthorhombic structure of Bi_2S_3 , since the positions of these energies, are specific to this particular site [35, 46] **Figure 3(b)** shows the unit cell with orthorhombic structure and the $\text{Bi}_{2-x}\text{Cr}_x\text{S}_3$ NCs with interstitial doping Cr^{3+} ions in a distorted octahedral symmetry. The bands identified in the spectral range of the visible in the OA spectra of **Figure 3(a)**, are assigned the spin allowed and forbidden transitions ${}^4\text{A}_2({}^4\text{F}) \rightarrow {}^2\text{E}_g({}^2\text{G})$ (1,79 eV), ${}^4\text{A}_2({}^4\text{F}) \rightarrow {}^2\text{T}_1({}^2\text{G})$ (1,86 eV), ${}^4\text{A}_{2g}({}^4\text{F}) \rightarrow {}^4\text{T}_{2g}({}^4\text{F})$ (1,94 eV), ${}^4\text{A}_{2g}({}^4\text{F}) \rightarrow {}^2\text{T}_{2g}({}^2\text{G})$ (2,59 eV), e ${}^4\text{A}_2({}^4\text{F}) \rightarrow {}^4\text{T}_1({}^4\text{F})$ (2,82 eV). Such energy states are a consequence of the strength of the crystal field ($\Delta = 15877 \text{ cm}^{-1}$) and the Racah parameter of interelectronic repulsion ($B = 665 \text{ cm}^{-1}$), based on the Tanabe-Sugano diagram d^3 octahedral (Oh) for $C/B = 4.5$ [46].

Therefore, the excited states of the coordination crystal field $[\text{CrS}_6]^{-9}$ are located within the energy band gap (2.95 eV) of the absorption associated with the excitonic transition of the $\text{Bi}_{2-x}\text{Cr}_x\text{S}_3$ NCs. The blueshift observed at the OA band edge for the $\text{Bi}_{2-x}\text{Cr}_x\text{S}_3$ NCs (2.95 eV) in relation to the corresponding intrinsic semiconductor (2.86 eV), results in sp-d exchange interactions between electrons confined in states of quantum dots and localized states partially filled with Cr^{3+} ions. The quantum size of the $\text{Bi}_{2-x}\text{Cr}_x\text{S}_3$ NCs does not change with the increase of Cr incorporation in the samples. **Figure 3(b)** shows an illustration of the $\text{Bi}_{2-x}\text{Cr}_x\text{S}_3$ NCs with quantum dot properties as a function of the x concentration of Cr^{3+} ions at octahedral sites.

$\text{Bi}_{2-x}\text{Cr}_x\text{S}_3$ NCs ($x = 0.10$) embedded in SNAB glass matrix with an average size of 10 nm are shown in the TEM image of **Figure 3(c)**. The distance $d_{210} = 0.325 \text{ nm}$ attributed to the crystal plane (210), shows the preserved orthorhombic structure for NCs Bi_2S_3 . The X-ray diffraction measurements for $\text{Bi}_{2-x}\text{Cr}_x\text{S}_3$ NCs ($x = 0.00$ and 0.05) confirm the standard peaks of the orthorhombic crystal system of the bismuthinite mineral (RRUFF ID: R070533.9). In the inset of **Figure 3(d)**, a shift to smaller angles (2θ) of the diffraction peak (210) is shown, as the Cr concentration increases from $x = 0.00$ to $x = 0.05$. The shift in the diffraction peak caused by a change in the lattice constant due to the substitute Bi^{3+} ions by Cr^{3+} in the orthorhombic crystal structure of Bi_2S_3 . The intensity of the XRD peaks increases with the xCr concentration. However, the structure preserved due to the non-saturation of the Cr doping concentration in the $\text{Bi}_{2-x}\text{Cr}_x\text{S}_3$ NCs.

1.4 Nickel-doped ZnTe nanocrystals embedded in host glass matrix

The incorporation of transition metal ions into wide energy gap semiconductors, as ZnTe ($E_g = 2.26 \text{ eV}$), [47] creates intermediate energy states between the valence and conduction bands in these host semiconductors, [48] allowing the manipulation of their magnetic and optical properties, [49] which in turn governs sp-d spin interaction between carriers and magnetic ions. Although Ni-doped ZnTe NCs are currently synthesized in various methods, [50, 51] some possible applications require nanoparticles to be embedded in highly stable, robust, and transparent host materials, as the glass systems. In this context, we present a very effective method for the growth of Ni^{2+} ion-doped ZnTe NCs in a glass system using the fusion nucleation method.

Figure 4 presents optical absorption (OA) spectra in the range of 250 nm - 1800 nm (a) and EPR spectra (b), of samples containing $Zn_{1-x}Ni_xTe$ NCs, with Ni-concentrations ranging from $x = 0.000$ to $x = 0.100$.

Already the **Figure 4(c)** shows TEM images of glass samples containing $Zn_{1-x}Ni_xTe$ NCs, with concentrations $x = 0.00$ and $x = 0.05$. Optical absorption spectra confirm the substitutional incorporation of Ni^{2+} ions in the ZnTe semiconductor lattice due to the absorption bands Ni^{2+} ion and the redshift from 3.10 eV (400 nm) to 2.85 eV (435 nm), when x ranges from 0.00 to 0.10. This redshift is related to the sp-d exchange interaction between the d band localized electrons of the Ni^{2+} transition

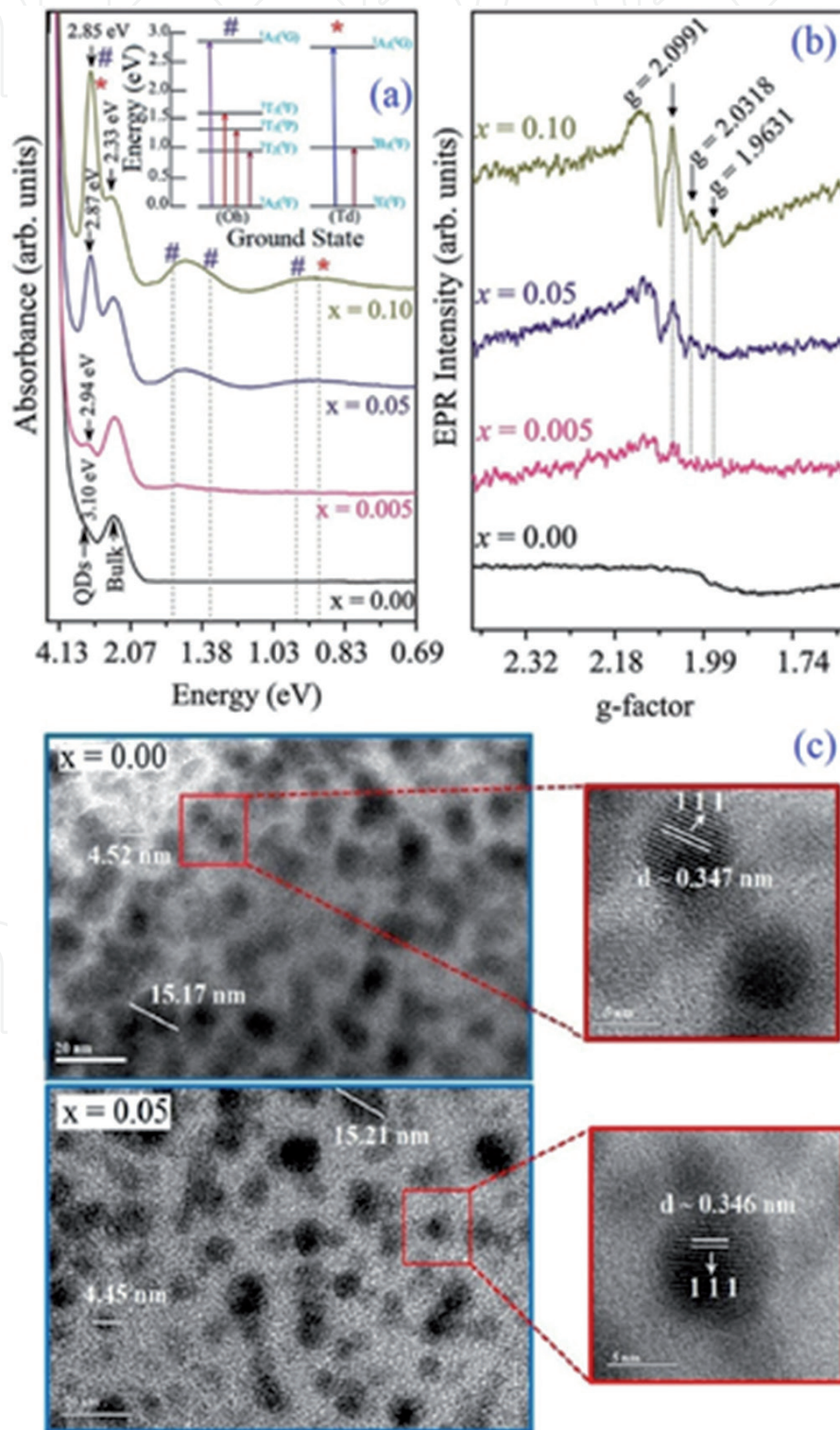


Figure 4. (a) Optical absorption (b) EPR spectra of samples containing $Zn_{1-x}Ni_xTe$ NCs, with Ni-concentrations ranging from $x = 0.000$ to $x = 0.100$. In (c) TEM images for concentrations $x = 0.00$ and $x = 0.05$.

metal ions and the sp. sub-levels electrons of the ZnTe host semiconductor, with increasing Ni concentration [51]. Transmission electronic microscopy (TEM) images were used to determine the NCs sizes, exhibiting quantum dots and bulk morphologies. It also revealed that the lattice parameter was not affected by higher concentrations of Ni doping. Ni^{2+} and Zn^{2+} have very similar ionic radii. Electron paramagnetic resonance spectra display resonance lines that confirm the substitutional incorporation ($g = 2.0991$) and also the presence of Ni^{2+} ions at vacancy sites ($g \approx 2.0023$) of the ZnTe lattice [52, 53].

Therefore, a more extensive investigation of the properties of ZnTe structures doped with Ni^{2+} ions could lead to novel technological applications in spintronic devices, as a magnetic field acting on the spin of the unpaired electrons would allow simultaneous use of spin, electronic and optical properties.

1.5 Manganese-doped CdTe nanocrystals embedded in host glass matrix

Cadmium chalcogenides doped with small amounts of magnetic impurities, such as manganese (Mn^{2+}) ions, called diluted magnetic semiconductors (DMS), have been extensively studied due to their significant magneto-optical properties [54–57]. In view of these interesting properties, In this section, we will comment in particular on Cadmium Telluride (CdTe) doped with Mn^{2+} ions [58, 59].

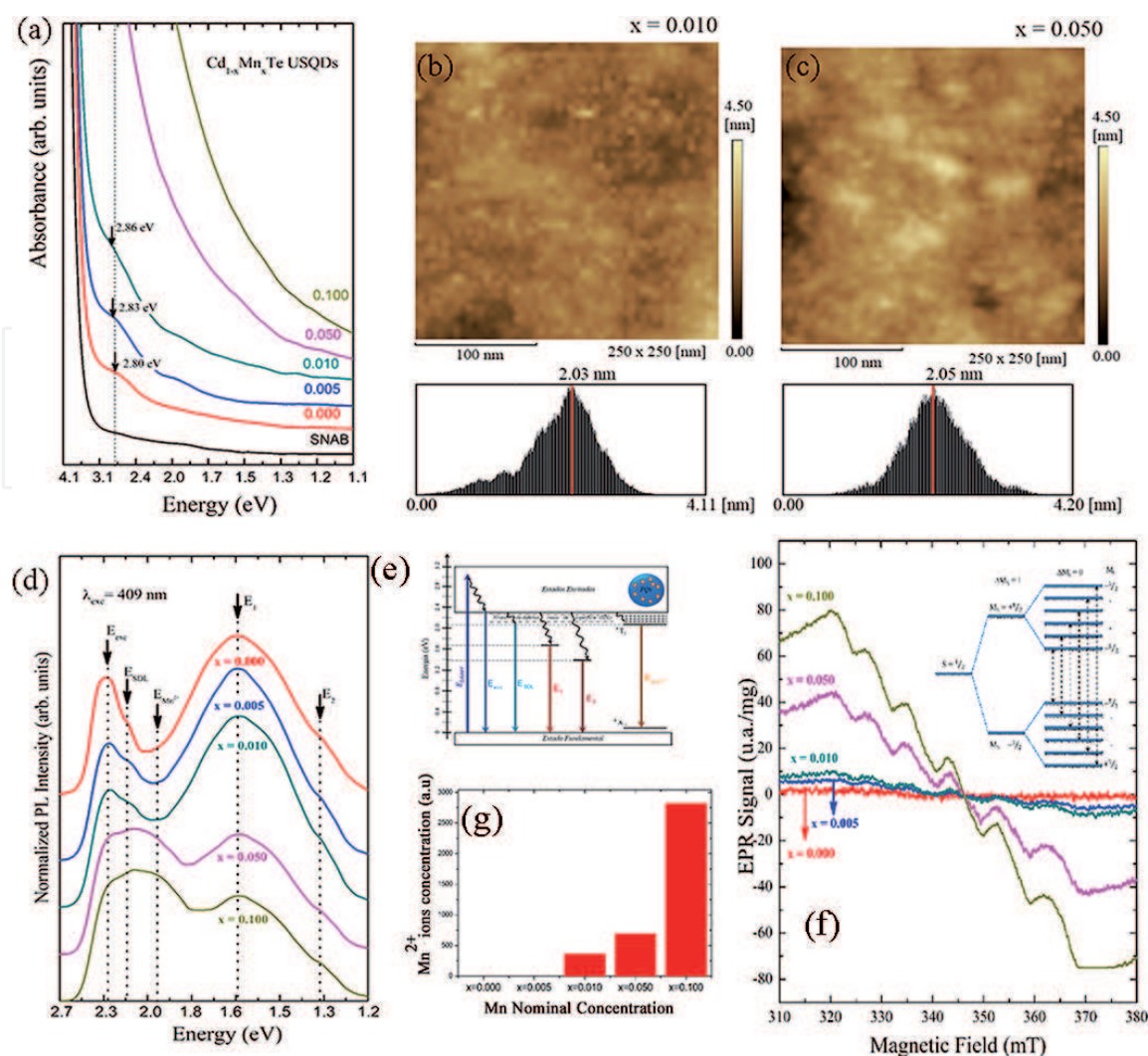
Figure 5(a) shows the optical absorption (OA) bands of CdTe ultra-small quantum dots (USQDs). As the concentration increases, there is a blueshift with an increase in magnetic doping, as indicated by the arrows: 2.87 eV ($x = 0.005$); 2.90 eV ($x = 0.010$); 2.92 eV ($x = 0.050$) and 2.94 eV ($x = 0.100$) [60]. The blueshift provides strong evidence that Mn^{2+} ions have actually been incorporated into the CdTe USQDs, which will be confirmed by the Electronic Paramagnetic Resonance (EPR) spectra.

The confirmation of the formation of the USQDs and the size distribution is confirmed in Atomic Force Microscopy (AFM) images, shown in **Figure 5(b)** and **(c)**. It is observed in the histograms of the topographic images that there was no relative change in the mean radius of the USQDs with the increase in manganese concentration.

In the luminescence spectra, **Figure 5(d)**, it is observed that with the increase in the concentration of manganese, there is an increase in the intensities of the emission bands centered around 564 nm (2.19 eV) and 617 nm (2.01 eV), attributed, respectively, to the levels of surface defects (E_{SDL}) and Mn^{2+} ions ($E_{\text{Mn}^{2+}}$). In addition, there is a decrease in the intensity of emissions related to vacancies E1 and E2, located around 753 nm (1.65 eV) and 892 nm (1.39 eV). $E_{\text{Mn}^{2+}}$ emission occurs between levels ${}^4T_1 \rightarrow {}^6A_1$, which is characteristic of the d orbital of Mn^{2+} ions when substitutionally incorporated in semiconductors II-VI [61].

Mn^{2+} ions can be substitutionally incorporated at two different sites: one in the nucleus (named as SI) [62] and another near the surface of the USQDs (named as SII) [58]. This emission ($E_{\text{Mn}^{2+}}$) is suppressed when the Mn^{2+} ions are incorporated into the USQDs' SII site [61]. Thus, the presence of $E_{\text{Mn}^{2+}}$ emission for higher concentrations of manganese confirms that Mn^{2+} ions are also incorporated in SI. On the other hand, the decrease in E1 and E2 emissions with the increase in manganese concentration shows that Mn^{2+} ions are replacing vacancies in $\text{Cd}_{1-x}\text{Mn}_x\text{Te}$ USQDs. All of these emissions are represented in the energy diagram in **Figure 5(e)**.

In the EPR spectra of the doped samples, the presence of the six lines is observed, which confirms that the Mn^{2+} ions are incorporated in the crystalline structure of the CdTe USQDs, replacing the Cd^{2+} sites, confirming that the grown structures are $\text{Cd}_{1-x}\text{Mn}_x\text{Te}$ USQDs (**Figure 5(f)**) [58]. The increase in the concentration of Mn^{2+} ions causes an increase in the intensity of the bottom lines. This effect is attributed to the dipole interactions between Mn-Mn. **Figure 5(g)** shows


Figure 5.

(a) Optical absorption spectra (b, c) AFM images, (d) Luminescence spectra, (e) Energy Diagram (f) EPR spectra, (g) Mn^{2+} ions Concentration of samples containing $Cd_{1-x}Mn_xTe$ UPNCs, with Mn-concentrations ranging from $x = 0.000$ to $x = 0.100$.

the estimate of the relative concentrations of Mn^{2+} ions for samples containing $Cd_{1-x}Mn_xTe$ USQDs with $x = 0.010$, 0.050 and 0.100 . It is observed that the increase in the concentration of manganese results in an increase in the concentration of Mn^{2+} ions inserted in the CdTe USQDs. Therefore, these results confirm the growth of $Cd_{1-x}Mn_xTe$ USQDs.

2. Conclusion

Therefore, this chapter shows how the incorporation of transition metals in nanocrystals can change their physical, chemical, and biological properties. In addition, depending on the application, these nanocrystals may be in powder or host glass systems. Interestingly, the doping with iron ions in the ZnO NCs did not change for malachite green degradation in relation of ZnO NCs. However, the doping with copper ions in ZnO NCs improved in the biocompatibility of ZnO NCs. Regarding physical properties, the incorporation of transition metals in semiconductors, allows the emergence of the magneto-optical properties as shown in nanocrystals doped with manganese, chromium or nickel ions, and their manipulation depend on the concentration and heat treatment when embedded in glass matrices.

Acknowledgements

This work was supported by grants of CNPq, CAPES, and FAPEMIG.

Conflict of interest

The authors declare no conflict of interest.

Author details

Anielle C.A. Silva^{1,2*}, Jerusa M. de Oliveira³, Luciana R.S. Floresta^{1,3},
Matheus V. da Silva^{1,4}, José L. da S. Duarte⁴, Karolina B. da Silva^{1,4},
Eurípedes A. da Silva Filho⁵, Vinícius P. Bittar^{1,6}, Ana L.S. Borges^{1,6},
Guilherme L. Fernandes⁷, Alessandra S. Silva⁸, Éder V. Guimarães⁸, Ricardo S. Silva⁸,
Carmem L.P.S. Zanta⁴, Lucas Anhezini³ and Noelio O. Dantas¹

1 Laboratory of New Nanostructured and Functional Materials, Physics Institute, Federal University of Alagoas, Maceió, Alagoas, Brazil

2 Programa de Pós-Graduação da Rede Nordeste de Biotecnologia (RENORBIO), Federal University of Alagoas, Maceió, Alagoas, Brazil

3 Laboratory for in vivo Toxicity, Institute of Biological Sciences and Health, Federal University of Alagoas, Maceió, Alagoas, Brazil

4 Laboratory of Applied Electrochemistry, Institute of Chemistry and Biotechnology, Federal University of Alagoas, Maceió, Alagoas, Brazil

5 Laboratory of Genetic and Applied Microbiology, Institute of Biological Sciences and Health, Federal University of Alagoas, Maceió, Alagoas, Brazil

6 Institute of Biotechnology, Federal University of Uberlândia, Uberlândia, Minas Gerais, Brazil

7 Physics Institute, Federal University of Uberlândia, Uberlândia, Minas Gerais, Brazil

8 Instituto de Ciências Exatas, Naturais e Educação (ICENE), Departamento de Física, Federal University of Triângulo Mineiro, Uberaba, Minas Gerais, Brazil

*Address all correspondence to: acalmeida@fis.ufal.br and noelio@fis.ufal.br

IntechOpen

© 2021 The Author(s). Licensee IntechOpen. This chapter is distributed under the terms of the Creative Commons Attribution License (<http://creativecommons.org/licenses/by/3.0>), which permits unrestricted use, distribution, and reproduction in any medium, provided the original work is properly cited. 

References

- [1] Tolaymat, T., Genaidy, A., Abdelraheem, W., Dionysiou, D., and Andersen, C. (2017) The effects of metallic engineered nanoparticles upon plant systems: An analytic examination of scientific evidence. *Sci. Total Environ.*, 579, 93-106.
- [2] Nair, R., Varghese, S.H., Nair, B.G., Maekawa, T., Yoshida, Y., and Kumar, D.S. (2010) Nanoparticulate material delivery to plants. *Plant Sci.*, 179 (3), 154-163.
- [3] Khot, L.R., Sankaran, S., Maja, J.M., Ehsani, R., and Schuster, E.W. (2012) Applications of nanomaterials in agricultural production and crop protection: A review. *Crop Prot.*, 35, 64-70.
- [4] Faizan, M., Hayat, S., and Pichtel, J. (2020) Effects of Zinc Oxide Nanoparticles on Crop Plants: A Perspective Analysis, pp. 83-99.
- [5] Jiang, S., Lin, K., and Cai, M. (2020) ZnO Nanomaterials: Current Advancements in Antibacterial Mechanisms and Applications. *Front. Chem.*, 8, 580.
- [6] Czyżowska, A., and Barbasz, A. (2020) A review: zinc oxide nanoparticles—friends or enemies? *Int. J. Environ. Health Res.*, 1-17.
- [7] Kolodziejczak-Radzimska, A., and Jesionowski, T. (2014) Zinc oxide—from synthesis to application: A review. *Materials (Basel)*, 7 (4), 2833-2881.
- [8] Pappus, S.A., and Mishra, M. (2018) A drosophila model to decipher the toxicity of nanoparticles taken through oral routes. *Adv. Exp. Med. Biol.*, 1048 (February), 311-322.
- [9] Singh, S. (2019) Zinc oxide nanoparticles impacts: cytotoxicity, genotoxicity, developmental toxicity, and neurotoxicity. *Toxicol. Mech. Methods*, 29 (4), 300-311.
- [10] Dugershaw, B.B., Aengenheister, L., Hansen, S.S.K., Hougaard, K.S., and Buerki-Thurnherr, T. (2020) Recent insights on indirect mechanisms in developmental toxicity of nanomaterials. *Part. Fibre Toxicol.*, 17 (1), 1-22.
- [11] Reis, É. de M., de Rezende, A.A.A., Santos, D.V., de Oliveria, P.F., Nicolella, H.D., Tavares, D.C., Silva, A.C.A., Dantas, N.O., and Spanó, M.A. (2015) Assessment of the genotoxic potential of two zinc oxide sources (amorphous and nanoparticles) using the in vitro micronucleus test and the in vivo wing somatic mutation and recombination test. *Food Chem. Toxicol.*, 84, 55-63.
- [12] Sousa, C.J.A.A., Pereira, M.C., Almeida, R.J., Loyola, A.M., Silva, A.C.A.A., and Dantas, N.O. (2014) Synthesis and characterization of zinc oxide nanocrystals and histologic evaluation of their biocompatibility by means of intraosseous implants. *Int. Endod. J.*, 47 (5), 416-424.
- [13] Bharat, T.C., Shubham, Mondal, S., Gupta, H.S., Singh, P.K., and Das, A.K. (2019) Synthesis of doped zinc oxide nanoparticles: A review. *Mater. Today Proc.*, 11, 767-775.
- [14] Bhattacharya, P., and Neogi, S. (2019) Antibacterial properties of doped nanoparticles. *Rev. Chem. Eng.*, 35 (7), 861-876.
- [15] Fakhri, A., Pourmand, M., Khakpour, R., and Behrouz, S. (2015) Structural, optical, photoluminescence and antibacterial properties of copper-doped silver sulfide nanoparticles. *J. Photochem. Photobiol. B Biol.*, 149, 78-83.
- [16] Ong, C., Yung, L.Y.L., Cai, Y., Bay, B.H., and Baeg, G.H. (2015) *Drosophila*

melanogaster as a model organism to study nanotoxicity. *Nanotoxicology*, 9 (3), 396-403.

[17] Reiter, L.T., Potocki, L., Chien, S., Gribskov, M., and Bier, E. (2001) A systematic analysis of human disease-associated gene sequences in *Drosophila melanogaster*. *Genome Res.*, 11 (6), 1114-1125.

[18] Pandey, U.B., and Nichols, C.D. (2011) Human disease models in *Drosophila melanogaster* and the role of the fly in therapeutic drug discovery. *Pharmacol. Rev.*, 63 (2), 411-436.

[19] Benford, D.J., Hanley, A.B., Bottrill, K., Oehlschlager, S., Balls, M., Branca, F., Castegnaro, J.J., Hemminiki, K., Lindsay, D., and Schilter, B. (2000) Biomarkers as Predictive Tools in Toxicity Testing The. *ATLA*, 28, 119-131.

[20] Silva, R.S. da, Neto, E.S. de F., and Dantas, N.O. (2012) Optical, Magnetic, and Structural Properties of Semiconductor and Semimagnetic Nanocrystals, in *Nanocrystals - Synthesis, Characterization and Applications*.

[21] Dantas, N.O., and Neto, E.S. de F. (2012) Carrier Dynamics and Magneto-Optical Properties of Cd_{1-x}MnxS Nanoparticles, in *Nanocrystals - Synthesis, Characterization and Applications*.

[22] Jo, D.Y., Kim, D., Kim, J.H., Chae, H., Seo, H.J., Do, Y.R., and Yang, H. (2016) Tunable White Fluorescent Copper Gallium Sulfide Quantum Dots Enabled by Mn Doping. *ACS Appl. Mater. Interfaces*, 8 (19), 12291-12297.

[23] Sanchez, R.S., Binetti, E., Torre, J.A., Garcia-Belmonte, G., Striccoli, M., and Mora-Sero, I. (2014) All solution processed low turn-on voltage near infrared LEDs based on core-shell PbS-CdS quantum dots with inverted device structure. *Nanoscale*, 6 (15), 8551-8555.

[24] Munawar Basha, S., Rama subramanian, S., Rajagopalan, M., Kumar, J., Won Kang, T., Ganapathi Subramaniam, N., and Kwon, Y. (2011) Investigations on cobalt doped GaN for spintronic applications. *J. Cryst. Growth*, 318 (1), 432-435.

[25] Sabat, D., Patnaik, A., Ekka, B., Dash, P., and Mishra, M. (2016) Investigation of titania nanoparticles on behaviour and mechanosensory organ of *Drosophila melanogaster*. *Physiol. Behav.*, 167, 76-85.

[26] Ng, C.T., Yong, L.Q., Hande, M.P., Ong, C.N., Yu, L.E., Bay, B.H., and Baeg, G.H. (2017) Zinc oxide nanoparticles exhibit cytotoxicity and genotoxicity through oxidative stress responses in human lung fibroblasts and *Drosophila melanogaster*. *Int. J. Nanomedicine*, 12, 1621-1637.

[27] Han, H., Sheng, Z., and Liang, J. (2006) A novel method for the preparation of water-soluble and small-size CdSe quantum dots. *Mater. Lett.*, 60 (29-30), 3782-3785.

[28] Baeg, E., Sooklert, K., and Sereemasun, A. (2018) Copper oxide nanoparticles cause a dose-dependent toxicity via inducing reactive oxygen species in drosophila. *Nanomaterials*, 8 (10).

[29] Zheng, F., Gonçalves, F.M., Abiko, Y., Li, H., Kumagai, Y., and Aschner, M. (2020) Redox toxicology of environmental chemicals causing oxidative stress. *Redox Biol.*, 34 (February), 101475.

[30] Uryu, O., Ameku, T., and Niwa, R. (2015) Recent progress in understanding the role of ecdysteroids in adult insects: Germline development and circadian clock in the fruit fly *Drosophila melanogaster*. *Zool. Lett.*, 1 (1), 1-9.

[31] Yamanaka, N., Marqués, G., and O'Connor, M.B. (2015)

Vesicle-Mediated Steroid Hormone Secretion in *Drosophila melanogaster*. *Cell*, 163 (4), 907-919.

[32] da Silva, R., Silva, J., Rocha, V., Cano, N., Almeida Silva, A., and Dantas, N. Synthesis Process Controlled of Semimagnetic $\text{Bi}_{2-x}\text{Mn}_x\text{S}_3$ Nanocrystals in a Host Glass Matrix. *J. Phys. Chem. C*, 118 (32), 18730-18735.

[33] Silva, R., Mikhail, H., Guimarães, E., Gonçalves, E., Cano, N., and Dantas, N. (2017) Synthesis and Study of Fe-Doped Bi_2S_3 Semimagnetic Nanocrystals Embedded in a Glass Matrix. *Molecules*, 22 (7), 1142.

[34] Guimarães, E. V., Gonçalves, E.R., Lourenço, S.A., Oliveira, L.C., Baffa, O., Silva, A.C.A., Dantas, N.O., and Silva, R.S. (2018) Concentration effect on the optical and magnetic properties of Co^{2+} -doped Bi_2S_3 semimagnetic nanocrystals growth in glass matrix. *J. Alloys Compd.*, 740, 974-979.

[35] Guimarães, É. V., Mikhail, H.D., Silva, A.C.A., Dantas, N.O., and Silva, R.S. (2020) Investigations of structural and optical properties of $\text{Bi}_{2-x}\text{Cr}_x\text{S}_3$ nanocrystals embedded in host glass. *Mater. Lett.*, 265.

[36] Han, D., Du, M.H., Dai, C.M., Sun, D., and Chen, S. (2017) Influence of defects and dopants on the photovoltaic performance of Bi_2S_3 : First-principles insights. *J. Mater. Chem. A*, 5 (13), 6200-6210.

[37] Ganose, A.M., Savory, C.N., and Scanlon, D.O. (2017) Beyond methylammonium lead iodide: prospects for the emergent field of ns^2 containing solar absorbers. *Chem. Commun.*, 53 (1), 20-44.

[38] Guo, D., Hu, C., and Zhang, C. (2013) First-principles study on doping and temperature dependence of thermoelectric property of Bi_2S_3

thermoelectric material. *Mater. Res. Bull.*, 48 (5), 1984-1988.

[39] Ge, Z.H., Qin, P., He, D., Chong, X., Feng, D., Ji, Y.H., Feng, J., and He, J. (2017) Highly Enhanced Thermoelectric Properties of $\text{Bi}/\text{Bi}_2\text{S}_3$ Nanocomposites. *ACS Appl. Mater. Interfaces*, 9 (5), 4828-4834.

[40] Konstantatos, G., Levina, L., Tang, J., and Sargent, E.H. (2008) Sensitive solution-processed Bi_2S_3 nanocrystalline photodetectors. *Nano Lett.*, 8 (11), 4002-4006.

[41] Li, Y., Zhang, Y., Lei, Y., Li, P., Jia, H., Hou, H., and Zheng, Z. (2012) In situ fabrication of Bi_2S_3 nanocrystal film for photovoltaic devices. *Mater. Sci. Eng. B Solid-State Mater. Adv. Technol.*, 177 (20), 1764-1768.

[42] Uddin, I., Ahmad, A., Ahmad Siddiqui, E., Hasanur Rahaman, S., and Gambhir, S. (2016) Biosynthesis of Fluorescent Bi_2S_3 Nanoparticles and their Application as Dual-Function SPECT-CT Probe for Animal Imaging. *Curr. Top. Med. Chem.*, 16 (18), 2019-2025.

[43] Lundegaard, L.F., Makovicky, E., Boffa-Ballaran, T., and Balic-Zunic, T. (2005) Crystal structure and cation lone electron pair activity of Bi_2S_3 between 0 and 10 GPa. *Phys. Chem. Miner.*, 32 (8-9), 578-584.

[44] Ramanery, F.P., Mansur, A.A.P., Mansur, H.S., Carvalho, S.M., and Fonseca, M.C. (2016) Biocompatible Fluorescent Core-Shell Nanoconjugates Based on Chitosan/ Bi_2S_3 Quantum Dots. *Nanoscale Res. Lett.*, 11 (1), 1-12.

[45] Riley, D.J., Waggett, J.P., and Upul Wijayantha, K.G. (2004) Colloidal bismuth sulfide nanoparticles: A photoelectrochemical study of the relationship between bandgap and particle size. *J. Mater. Chem.*, 704-708.

- [46] Araujo, C.M., Mikhail, H.D., Guimarães, E. V., Rastrello, L.R., Cano, N.F., Silva, A.C.A., Dantas, N.O., and Silva, R.S. (2020) Optical, structural and magnetic characterization of $\text{Bi}_{2-x}\text{Cr}_x\text{Te}_3$ nanocrystals in oxide glass. *Mater. Chem. Phys.*, 241.
- [47] Alivisatos, A.P. (1996) Semiconductor Clusters, Quantum Nanocrystals, and Quantum Dots. *Science* (80-.), 271 (5251), 933-937.
- [48] Norris, D.J., Efros, A.L., and Erwin, S.C. (2008) Doped nanocrystals. *Science* (80-.), 28 (319), 1776-9.
- [49] Karan, N.S., Sarma, D.D., Kadam, R.M., and Pradhan, N. (2010) Doping transition metal (Mn or Cu) ions in semiconductor nanocrystals. *J. Phys. Chem. Lett.*, 1 (19), 2863-2866.
- [50] Mahmood, A., Rashid, R., Aziz, U., Shah, A., Ali, Z., Raza, Q., and Ashraf, T. (2015) Structural and optical properties of $\text{Zn}_{1-x}\text{Ni}_x\text{Te}$ thin films prepared by electron beam evaporation technique. *Prog. Nat. Sci. Mater. Int.*, 25 (1), 22-28.
- [51] Chaik, M., Ben Moumen, S., Bouferra, R., Outzourhit, A., and Essaleh, L. (2020) Analysis of the electrical impedance spectroscopy measurements of $\text{ZnTe}:\text{Ni}$ thin film deposited by R-F sputtering. *Superlattices Microstruct.*, 137.
- [52] Silva, A.S., Figueiredo, L.C., de Souza, P.E.N., Morais, P.C., Pelegrini, F., and Dantas, N.O. (2020) Effect of Ni^{2+} ions concentration on the local crystal field of $\text{Zn}_{1-x}\text{Ni}_x\text{Te}$ nanocrystals. *Chem. Phys. Lett.*, 750 (March).
- [53] Premkumar, H.B., Sunitha, D. V., Nagabhushana, H., Sharma, S.C., Nagabhushana, B.M., Shivakumara, C., Rao, J.L., and Chakradhar, R.P.S. (2013) Synthesis, characterization, EPR, photo and thermoluminescence properties of $\text{YAlO}_3:\text{Ni}^{2+}$ nanophosphors. *J. Lumin.*, 135, 105-112.
- [54] Freitas Neto, E.S., Da Silva, S.W., Morais, P.C., and Dantas, N.O. (2013) Multiphonon Raman scattering in coupled $\text{Cd}_{1-x}\text{Mn}_x\text{S}$ nanoparticles: Magnetic doping and thermal annealing. *J. Phys. Chem. C*, 117 (1), 657-662.
- [55] Neto, E.S.F., Dantas, N.O., and Lourenço, S.A. (2012) Carrier dynamics in the luminescent states of $\text{Cd}_{1-x}\text{Mn}_x\text{S}$ nanoparticles: Effects of temperature and x-concentration. *Phys. Chem. Chem. Phys.*, 14, 1493-1501.
- [56] Neto, E.S.F., Dantas, N.O., Neto, N.M.B., Guedes, I., and Chen, F. (2011) Control of luminescence emitted by $\text{Cd}_{1-x}\text{Mn}_x\text{S}$ nanocrystals in a glass matrix: X concentration and thermal annealing. *Nanotechnology*, 22 (10).
- [57] Dantas, N.O., De Lima Fernandes, G., Baffa, O., Gómez, J.A., and Almeida Silva, A.C. (2014) $\text{Cd}_{1-x}\text{Mn}_x\text{Te}$ ultrasmall quantum dots growth in a silicate glass matrix by the fusion method. *Appl. Phys. Lett.*, 105 (13).
- [58] Dantas, N.O., De Lima Fernandes, G., Baffa, O., Gómez, J.A., and Almeida Silva, A.C. (2014) $\text{Cd}_{1-x}\text{Mn}_x\text{Te}$ ultrasmall quantum dots growth in a silicate glass matrix by the fusion method. *Appl. Phys. Lett.*, 105 (13).
- [59] Dantas, N.O., Fernandes, G.L., Baffa, O., Gómez, J.A., and Silva, A.C.A. (2015) Controlling Densities of Manganese Ions and Cadmium Vacancies in $\text{Cd}_{1-x}\text{Mn}_x\text{Te}$ Ultrasmall Quantum Dots in a Glass Matrix: x -Concentration and Thermal Annealing. *J. Phys. Chem. C*, 119 (30), 17416-17420.
- [60] Dantas, N.O., Neto, E.S.F., Silva, R.S., Jesus, D.R., and Pelegrini, F. (2008) Evidence of $\text{Cd}_{1-x}\text{Mn}_x\text{S}$ nanocrystal growth in a glass matrix

by the fusion method. *Appl. Phys. Lett.*,
93 (19), 193115.

[61] Zhou, H., Hofmann, D.M., Alves,
H.R., and Meyer, B.K. (2006)
Correlation of Mn local structure and
photoluminescence from CdS:Mn
nanoparticles. *J. Appl. Phys.*, 99
(10), 103502.

[62] Ayta, W.E.F., Dantas, N.O., Silva,
A.C.A., and Cano, N.F. (2010) First
evidence of crystalline KHSO₄:Mn
grown by an aqueous solution method
and the investigation of the effect of
ionizing radiation exposure. *J. Cryst.
Growth*, 312 (4), 563-567.

IntechOpen